

Multiple Bloch surface wave excitation with gratings

Original

Multiple Bloch surface wave excitation with gratings / Lewis, Asilevi; Descrovi, Emiliano; Pesonen, Henri; Roussey, Matthieu; Turunen, Jari. - In: JOURNAL OF THE EUROPEAN OPTICAL SOCIETY. RAPID PUBLICATIONS. - ISSN 1990-2573. - 20:1(2024). [10.1051/jeos/2024007]

Availability:

This version is available at: 11583/2986256 since: 2024-02-23T09:02:12Z

Publisher:

EDP Sciences

Published

DOI:10.1051/jeos/2024007

Terms of use:

This article is made available under terms and conditions as specified in the corresponding bibliographic description in the repository

Publisher copyright

EDP preprint/submitted version e/o postprint/Author's Accepted Manuscript

© EDP Sciences. The original publication is available at

https://jeos.edpsciences.org/articles/jeos/full_html/2024/01/jeos20230066/jeos20230066.html

(Article begins on next page)

Multiple Bloch surface wave excitation with gratings

Atsu L. Asilevi^{1,*}, Emiliano Descrovi², Henri Pesonen³, Matthieu Roussey¹, and Jari Turunen¹

¹Center for Photonics Sciences, Department of Physics and Mathematics, University of Eastern Finland, P.O. Box 111, 80101 Joensuu, Finland

²Dipartimento di Scienza Applicata e Tecnologia, Politecnico di Torino, 10129 Torino, Italy

³Dispelix Oy, Yliopistokatu 7, FI-80130 Joensuu, Finland

*Corresponding author: lewisa@uef.fi

Abstract. We study the coupling of a finite number of Bloch surface waves (BSWs) propagating in different directions at the surface of a dielectric multilayer. These surface waves arise from a set of diffraction orders associated to a grating on the bottom surface of the substrate that is illuminated by a normally incident beam. Simultaneous excitation of multiple BSWs is possible with a set of diffraction orders having the same radial spatial frequency. Using rigorous electromagnetic theory, we design gratings for simultaneous excitation of two, four and six BSWs propagating in directions separated by π , $\pi/2$ and $\pi/3$ azimuthal intervals, respectively.

Keywords: Evanescent waves, Surface Electromagnetic Waves, Bloch Surface Waves, Multiple Bloch Surface Waves, MBSWs.

1 Introduction

Surface Electromagnetic Waves (SEW) represent an interesting option for controlling optical signals on miniaturized chips for integrated optics and sensing applications. Surface Plasmon Polaritons (SPP) are probably the most widely known SEWs, but they exhibit inherent issues related to the ohmic losses introduced by the metallic materials involved. As an alternative, SEWs sustained by dielectric multilayers (ML) have attracted a growing interest in the past decade. This kind of SEW [1] are also referred to as Bloch Surface Waves (BSWs) [2] to highlight the role of the underlying periodic multilayer structure required for their existence. BSWs offer several advantages as compared to SPPs, such as a wide spectral tunability and low losses thanks to the large choice of transparent dielectric materials available for multilayer manufacturing. In addition, BSWs can be either TE- or TM-polarized [3,4], depending on the multilayer design. Their excitation by pulsed fields has also been recently studied numerically [5].

Being surface waves, BSWs are evanescent in the medium above the multilayer surface. The coupling with free-space radiation in a BSW-based device is therefore critical as it must provide momentum matching beyond the light-line. In most of the applications proposed so far, BSW coupling is performed by means of bulky prisms, either in Kretschmann or Otto configuration [6]. However, more sophisticated approaches have been recently implemented, involving, for example, the use of individual scatterers [7–9] or miniature prisms [10] placed onto the multilayer surface. Another promising option is represented by integrating diffraction gratings within the BSW-supporting structure [11]. This has been done mainly in two different ways: with the grating being fabricated on top of the multilayer [12–14] or buried beneath the multilayer [15]. In the first case, the multilayer is substantially planar, with the ex-

ception of the top layer, where the grating unavoidably perturbs the dispersion of the BSW mode (dielectric loading/unloading effect). In the second case, the grating is fabricated on the substrate surface prior to the multilayer deposition, which occurs on the same side. The multilayer itself results to not be perfectly planar because it (partially) conforms to the underlying corrugation. In both configurations, the BSW dispersion is altered by the presence of the grating, which may lead to some difficulties regarding the precise control of optical functions of complex, possibly resonating, BSW-based architectures.

We propose an alternative approach on diffractive coupling for BSWs, with gratings fabricated on the bottom surface of a transparent substrate having the multilayer deposited on the top surface. In particular, we explore the possibility of using two-dimensional gratings to simultaneously couple BSWs propagating in more than two directions by exploiting the momentum distribution of several diffraction orders. Once the mode dispersion of the multilayer is known, our approach facilitates BSW coupling in a controllable way, as far as wavelengths/numbers and propagation directions are concerned. The directional coupling of BSWs has been already tackled in a few previous articles [16–18], although never considered for multiple directions at once. When the optical path through the substrate is also taken into account, our approach allows a predictable control onto the coupling locations of BSWs launched in different directions.

The present paper is composed as follows. We begin, in Sec. 2, by introducing the grating-based BSW excitation principle and the assumed geometrical configuration. The theoretical framework for grating design, for which we use a rigorous technique known as the Fourier Modal Method (FMM) [19], is described in Sec. 3. The design process is analogous with the synthesis of grating-based mul-

63 tiple free-space beam splitters [20], but here we need to account
64 for the BSW excitation conditions and the polarization state of the
65 input wave. In Sec. 4, we first consider BSW stack design, pro-
66 viding a ‘benchmark’ stack employed in the rest of the work, and
67 then cover the design of linear gratings for simultaneous excitation
68 of two counter-propagating BSWs. Such designs are extended in
69 Sec. 5 to two-dimensional periodic gratings for excitation of either
70 four or six BSWs propagating at 90° or 60° intervals along the
71 stack, respectively. After a discussion presented in Sec. 6, conclu-
72 sions are drawn in Sec. 7.

73 2 Excitation principle and geometry

74 Figure 1 illustrates the geometry for the simplest case of excita-
75 tion of two counter-propagating BSWs. A flat fused silica substrate
76 with refractive index $n_{\text{sub}} = 1.462$, such as a 0.5 mm or 3 mm-
77 thick SiO_2 plate, is illuminated by a normally incident monochro-
78 matic beam (wavelength λ_0) from the medium underneath (air).
79 A linear grating, with period d of the order of λ_0 , provided on
80 the air-substrate surface, splits the beam into three transmitted or-
81 ders propagating within the substrate: the zeroth order $m = 0$ and
82 the first diffracted orders $m = \pm 1$. The orders $m = \pm 1$ propa-
83 gate in directions θ_{+1} and θ_{-1} given by $\sin \theta_{\pm 1} = \pm \lambda_0 / n_{\text{sub}} d$
84 towards the multilayer stack on the top surface of the substrate.
85 If $|\theta_{\pm 1}|$ matches the Kretschmann-incidence BSW excitation an-
86 gle θ_{BSW} for the given wavelength and polarization state (TE
87 or TM), two counter-propagating BSWs are generated simultane-
88 ously. The excitation is efficient as long as the angular spectrum
89 of each diffracted order, which defines the beam divergence, falls
90 essentially within the (stack-dependent) BSW momentum band-
91 width. The polarization state of illumination affects the coupling
92 significantly; we will consider only BSW excitation in TE polar-
93 ization, which generally requires a smaller number of stack layers
94 than TM-polarized BSW excitation.

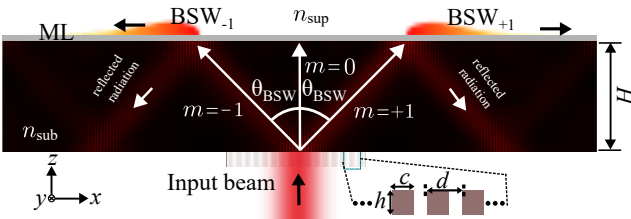


Figure 1: Principle of MBSW generation: the two-beam case. A binary linear surface-relief grating defined by period d , ridge width c , and ridge height h on the bottom of a substrate of thickness H splits the input beam into two diffracted orders $m = -1$ and $m = +1$, which excite BSWs on the top surface of the substrate by interaction with the multilayer stack (ML). We assumed $n_{\text{sub}} = 1.462$ and n_{sup} is air.

95 The parameters of the system are chosen such that the two BSWs
96 shown in Fig. 1 are spatially separated under finite-beam illumina-
97 tion. This feature can be useful in BSW-based platforms such as
98 interferometers [23] and integrated components [24]. First-order
99 diffracted beams are partially reflected at the top interface, thus
100 propagating back into the substrate. The reflected beams continue
101 to propagate according to multiple-reflection paths inside the sub-

strate unless they are extracted by means of diffusers or gratings.
103 At each reflection with the ML interface, coupling to BSW occurs.
104 Stated differently, BSWs are launched at different locations on the
105 ML surface each time the beam is incident on the bottom interface
106 of the dielectric stack, thus leading to the appearance of BSW inter-
107 ference effects unless the substrate thickness H is sufficiently large
108 to minimize spatial overlaps.

109 3 Theoretical framework

110 Let us consider a rectangularly periodic grating of period $d_x \times d_y$
111 in the cartesian xy coordinate system and assume a plane-wave
112 illumination (at frequency ω) normally incident onto the substrate
113 from air. In view of the grating equations, the wave vectors of the
114 propagating diffraction orders (m, n) in the substrate are

$$115 \mathbf{k}_{mn} = k_{xm} \hat{x} + k_{yn} \hat{y} + k_{zmn} \hat{z} \quad (1)$$

115 where

$$116 k_{xm} = mK_x = 2\pi m/d_x, \quad (2a)$$

$$117 k_{yn} = nK_y = 2\pi n/d_y, \quad (2b)$$

$$118 k_{zmn} = \sqrt{k_0^2 n_{\text{sub}}^2 - k_{xm}^2 - k_{yn}^2}, \quad (2c)$$

116 and $k_0 = \omega/c_0 = 2\pi/\lambda_0$ is the wave number in vacuum. After
117 defining the radial spatial frequency of the generic order (m, n) as

$$118 k_{\rho mn} = \sqrt{k_{xm}^2 + k_{yn}^2} = \sqrt{(mK_x)^2 + (nK_y)^2}, \quad (3)$$

118 the condition $k_{\rho mn} < k_0 n_{\text{sub}}$ identifies those diffraction orders
119 propagating within the substrate, the others being evanescent. If
120 we denote the refractive index of the superstrate by n_{sup} and as-
121 sume $n_{\text{sup}} < n_{\text{sub}}$, order (m, n) is evanescent in the superstrate
122 when $k_{\rho mn} > k_0 n_{\text{sup}}$. Considering BSW excitation, we are there-
123 fore interested in orders with radial spatial frequencies in the range
124 $k_0 n_{\text{sup}} < k_{\rho mn} < k_0 n_{\text{sub}}$. We are primarily interested in the near-
125 est neighbors of the zeroth transmitted order, while higher orders
126 are made evanescent by appropriate choices of d_x and d_y . In the il-
127 lustrative example presented in Fig. 2(a), orders $(m, n) = (-1, 0)$
128 and $(m, n) = (+1, 0)$ fall on the yellow line of radius $k_{\rho \text{BSW}}$,
129 which defines the BSW excitation condition dictated by the ML
130 design.

131 Following Ref. [21], we define the ‘exit plane’ of diffraction order
132 (m, n) as the plane containing the wave vector \mathbf{k}_{mn} and the unit
133 vector \hat{z} . Further, propagation angles θ_{mn} and ϕ_{mn} of the trans-
134 mitted orders, are defined as

$$135 k_{xm} = k_0 n_{\text{sub}} \sin \theta_{mn} \cos \phi_{mn}, \quad (4a)$$

$$136 k_{yn} = k_0 n_{\text{sub}} \sin \theta_{mn} \sin \phi_{mn}, \quad (4b)$$

$$137 k_{zmn} = k_0 n_{\text{sub}} \cos \theta_{mn}. \quad (4c)$$

135 as illustrated in Fig. 2(b). Here ϕ_{mn} is the azimuthal angle in the
136 range $[0, 2\pi)$, measured counter-clockwise from the k_x axis, and
137 θ_{mn} in the range $[0, \pi/2)$ is the propagation angle measured from

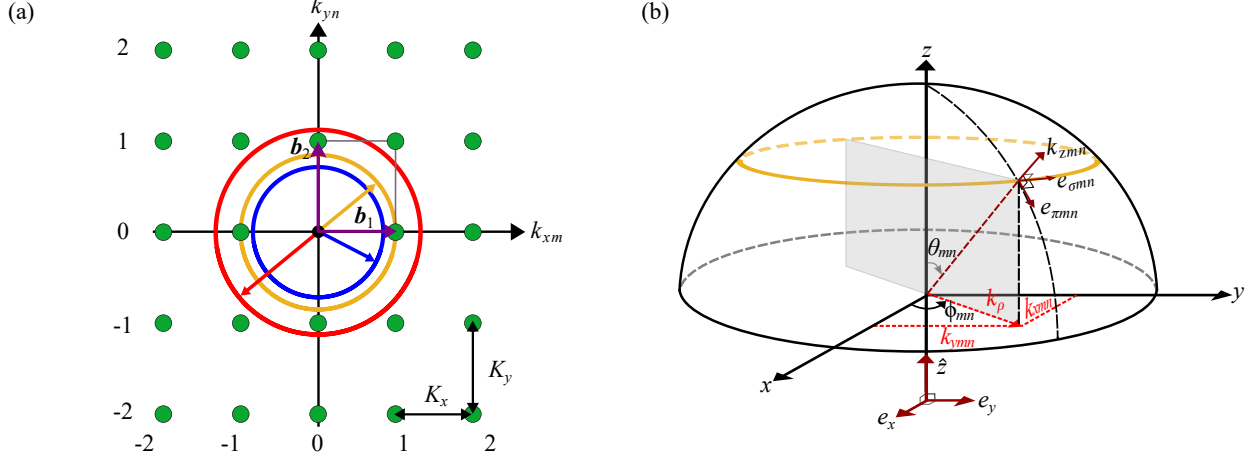


Figure 2: (a) Diffraction orders of a rectangular lattice in spatial-frequency representation at normal incidence. Diffraction orders are represented by dots at positions $k_{xm} = mK_x$, $k_{yn} = nK_y$. Blue and red circles represent the cut-off radial spatial frequencies $k_\rho = k_0 n_{\text{sub}}$ and $k_\rho = k_0 n_{\text{sup}}$, respectively, between which BSW excitation is possible. The yellow circle indicates the radial spatial frequency of BSW on a given ML. (b) Definition of the propagation angles (θ_{mn} , ϕ_{mn}) of a single transmitted diffracted order (m, n) in its exit plane (the grey rectangle) and the $\pi - \sigma$ basis of the diffracted electric field.

138 the k_z axis. It will prove convenient to use the so-called $\pi - \sigma$
 139 basis (or local TM/TE basis) to define the polarization states of the
 140 transmitted orders. As described in Ref. [21], this basis allows us
 141 to treat incident fields with any polarization state, including partial
 142 polarization. Here, however, we are mainly interested in either fully
 143 polarized or unpolarized illumination.

144 If the incident plane wave is fully polarized, we can use any suit-
 145 able rigorous grating analysis method (in our case FMM) to deter-
 146 mine the transverse Cartesian components e_{xmn} and e_{ymn} of the
 147 polarization vector for any transmitted order, as discussed shortly
 148 below. The longitudinal component of e_{mn} is fixed by Maxwell's
 149 divergence equation, which gives $\mathbf{k}_{mn} \cdot \mathbf{e}_{mn} = 0$ and

$$e_{zmn} = -\frac{1}{k_{zmn}} (k_{xm} e_{xmn} + k_{yn} e_{ymn}). \quad (5)$$

150 In the $\pi - \sigma$ basis the polarization state of any order is described
 151 by a two-dimensional vector $\mathbf{e}_{\pi\sigma mn} = [e_{\pi mn}, e_{\sigma mn}]^T$, where the
 152 π and σ components are explicitly given by

$$e_{\pi mn} = e_{xmn} \cos \theta_{mn} \cos \phi_{mn} + e_{ymn} \cos \theta_{mn} \sin \phi_{mn} \\ - e_{zmn} \sin \theta_{mn}, \quad (6a)$$

$$e_{\sigma mn} = -e_{xmn} \sin \phi_{mn} + e_{ymn} \cos \phi_{mn}. \quad (6b)$$

153 As shown in Fig. 2(b), the component $e_{\pi mn}$ lies in the exit plane,
 154 whereas $e_{\sigma mn}$ is perpendicular to it. Hence, they represent the TM
 155 and TE components of the electric field in the exit plane, respec-
 156 tively.

157 In diffraction by two-dimensionally periodic gratings, the polar-
 158 ization states of the transmitted (and reflected) diffracted orders
 159 generally depend on the state of input polarization. We represent
 160 the polarization vector of a (generally, elliptically polarized) unit-
 161 amplitude input plane wave as

$$\mathbf{e} = e_x \hat{\mathbf{x}} + e_y \hat{\mathbf{y}} = \hat{\mathbf{x}} \cos \alpha + \hat{\mathbf{y}} \sin \alpha \exp(i\delta), \quad (7)$$

162 normalized such that $\mathbf{e} = 1$. The effect of the grating on transmitted
 163 radiation can be analyzed by calculating (by FMM) the transmis-

164 sion coefficients

$$T_{xmn}^{(x)}, T_{ymn}^{(x)}, T_{xmn}^{(y)}, T_{ymn}^{(y)}, \quad (8)$$

165 for all diffraction orders, where the superscripts (x) and (y) re-
 166 fer to illumination by a purely x -polarized ($\mathbf{e} = \hat{\mathbf{x}}$) or y -polarized
 167 ($\mathbf{e} = \hat{\mathbf{y}}$) incident wave. The coefficients in Eq. (8) are precisely
 168 the complex vector amplitudes that appear in the Rayleigh plane-
 169 wave expansion of the field at the output plane of the grating; see,
 170 e.g., Eq. (5) in Ref. [20]. For an arbitrarily (fully) polarized incident
 171 wave the transverse electric-field components of the transmitted or-
 172 ders are [21]

$$e_{xmn} = T_{xmn}^{(x)} e_x + T_{xmn}^{(y)} e_y, \quad (9a)$$

$$e_{ymn} = T_{ymn}^{(x)} e_x + T_{ymn}^{(y)} e_y. \quad (9b)$$

173 The longitudinal components e_{zmn} are obtained from Eq. (5), and
 174 the $\pi - \sigma$ representation of each order is given by Eqs. (6). Since the
 175 input polarization state affects both the π and σ components, it can
 176 be used as a design degree of freedom in multiple-BSW excitation,
 177 in addition to the geometrical grating parameters.

178 It is customary to describe the state of polarization of a fully po-
 179 larized field by a 2×2 polarization matrix $\mathbf{J} = \mathbf{e}^* \mathbf{e}^T$ (Ref. [22],
 180 sec. 6.3.2). Explicitly, for the incident field,

$$\mathbf{J} = \begin{bmatrix} J_{xx} & J_{xy} \\ J_{yx} & J_{yy} \end{bmatrix} = \begin{bmatrix} |e_x|^2 & e_x^* e_y \\ e_y^* e_x & |e_y|^2 \end{bmatrix}, \quad (10)$$

181 where the asterisk denotes complex conjugation. Correspondingly,
 182 the polarization state of any transmitted order in the $\pi - \sigma$ basis is
 183 described by $\mathbf{J}_{\pi\sigma mn} = \mathbf{e}_{\pi\sigma mn}^* \mathbf{e}_{\pi\sigma mn}^T$ [21], explicitly

$$\mathbf{J}_{\pi\sigma mn} = \begin{bmatrix} J_{\pi\pi mn} & J_{\pi\sigma mn} \\ J_{\sigma\pi mn} & J_{\sigma\sigma mn} \end{bmatrix} = \begin{bmatrix} |e_{\pi mn}|^2 & e_{\pi mn}^* e_{\sigma mn} \\ e_{\sigma mn}^* e_{\pi mn} & |e_{\sigma mn}|^2 \end{bmatrix}. \quad (11)$$

184 The polarization states of the diffracted orders can also be charac-
185 terized by the Stokes parameters [21]

$$S_{0mn} = J_{\pi\pi mn} + J_{\sigma\sigma mn}, \quad (12a)$$

$$S_{1mn} = J_{\pi\pi mn} - J_{\sigma\sigma mn}, \quad (12b)$$

$$S_{2mn} = 2\Re(J_{\pi\sigma mn}), \quad (12c)$$

$$S_{3mn} = 2\Im(J_{\pi\sigma mn}), \quad (12d)$$

186 where \Re and \Im denote the real and imaginary parts. The nor-
187 malized forms of the Stokes parameters are defined as $s_{jmn} =$
188 S_{jmn}/S_{0mn} ($j = 1, 2, 3$), and the degree of polarization associ-
189 ated with order (m, n) is given by

$$P_{mn} = \sqrt{s_{1mn}^2 + s_{2mn}^2 + s_{3mn}^2}. \quad (13)$$

190 For a fully polarized incident wave, $P_{mn} = 1$ for all orders, even
191 though the values of the individual Stokes parameters generally de-
192 pend on order indices.

193 In addition to fully polarized illumination, we consider the opposite
194 extreme case of unpolarized illumination. The matrix \mathbf{J} for partially
195 polarized light is defined as $\mathbf{J} = \langle e^* e^T \rangle$, where the brackets denote
196 ensemble averaging over all polarization realizations. For unpolar-
197 ized illumination it has a diagonal form (Ref. [22], sec. 6.3.3)

$$\mathbf{J} = \frac{1}{2} \begin{bmatrix} 1 & 0 \\ 0 & 1 \end{bmatrix} \quad (14)$$

198 and the degree of input polarization is $P = 0$. The polarization ma-
199 trix associated with order (m, n) can be represented as an average

$$\mathbf{J}_{\pi\sigma mn} = \frac{1}{2} \left[\mathbf{J}_{\pi\sigma mn}^{(x)} + \mathbf{J}_{\pi\sigma mn}^{(y)} \right], \quad (15)$$

200 which remains diagonal because e_x and e_y are uncorrelated. How-
201 ever, since the grating treats these components differently, in gen-
202 eral $J_{\pi\pi mn} \neq J_{\sigma\sigma mn}$, implying that the individual orders become
203 partially polarized with $P_{mn} > 0$.

204 In standard beam splitting problems in resonance-domain diffrac-
205 tive optics [20] one is interested in the distribution of the diffraction
206 efficiencies of the propagating orders. Since we have normalized
207 the intensity of the incident field such that $S_0 = 1$, the diffraction
208 efficiencies are defined as [21]

$$\eta_{mn} = n_{\text{sub}} \cos \theta_{mn} S_{0mn}. \quad (16)$$

209 **In BSW excitation problem, the design goal is to maximize and**
210 **equalize the coupling of the incident field to a set of BSW modes**
211 **with the angle θ_{mn} equal to θ_{BSW} . If θ_{BSW} is the excitation angle**
212 **for TE polarization, the component $e_{\sigma mn}$ excites a BSW while**
213 **$e_{\pi mn}$ is non-resonant, and vice versa.**

214 We choose the geometry such that several diffraction orders have
215 the same radial spatial frequency $k_{\rho mn} = k_0 n_{\text{sub}} \sin \theta_{\text{BSW}}$, and
216 therefore lie on the yellow circle depicted in Fig. 2(a). The relative
217 amplitudes of the excited BSWs are determined by the σ -polarized

218 components $J_{\sigma\sigma mn}$ in TE polarization and $J_{\pi\pi mn}$ in TM polar-
219 ization. The fraction

$$\kappa_{mn} = J_{\sigma\sigma mn} / J_{\pi\pi mn} \quad (17)$$

220 provides the ratio of the coupled and uncoupled parts of the inci-
221 dent wave in BSW excitation.

222 4 Plane-wave design with linear gratings

223 As evident from the preceding discussion, the $\pi - \sigma$ representation
224 returns the BSW excitation problem to the basic TE or TM polar-
225 ized problem. In addition, since we assume a substrate thickness
226 $H \gg \lambda_0$, the evanescent parts of the diffracted fields above the
227 grating and the BSW field below the stack are spatially well sepa-
228 rated. Hence, we may treat the BSW stack design and the grating
229 design as two separate problems. In order to obtain an illustrative
230 stack design useful for our purposes, we fix $\lambda_0 = 514$ nm and pro-
231 vide a stack geometry sustaining BSWs at angles between the blue
232 and red lines in Fig. 2(a). The resulting stack can then be used to
233 design gratings for excitation of BSWs that lie on the yellow circle
234 in Fig. 2(a).

235

236 4.1 Multilayer stack design

237 Figure 3(a) shows the assumed stack structure, which consists of
238 N high/low (H/L) refractive index bilayers and a terminating top
239 (T) layer with refractive indices n_{H} , n_{L} , n_{T} and thicknesses h_{H} ,
240 h_{L} , h_{T} , respectively. To reduce the number of variable parameters,
241 we consider TE polarization, fix the number of bilayers to $N = 6$,
242 use refractive indices $n_{\text{H}} = 2.520$ (TiO₂), $n_{\text{L}} = 1.476$ (SiO₂),
243 $n_{\text{T}} = n_{\text{H}} = 2.520$. The thicknesses h_{H} , h_{L} , h_{T} are used to design
244 the stack such that the BSW resonance occurs at an angle θ_{mn} in
245 the exit plane.

246 Figure 3(b) shows the design results. The horizontal axis is
247 $k_x/k_0 = n_{\text{sub}} \sin \theta_{mn} = n_{\text{eff}}$, where n_{eff} can be interpreted as
248 the effective index of the stack. The plotting range starts from the
249 critical angle of BSW generation and extends to $k_x/k_0 n_{\text{sub}}$, i.e., it
250 spans the region between the blue and red circles in Fig. 2(a). As
251 n_{eff} increases, the BSW becomes increasingly buried within the
252 multilayer and acts less like a surface mode. At the same time, all
253 layer thicknesses show a monotonically increasing trend.

254

255 4.2 Two-way splitting

256 As illustrated in Fig. 1, the coupling of two counter-propagating
257 BSWs is possible with linear gratings ($d_x = d$, $d_y = \infty$). The
258 exit plane of both orders, $(m, n) = (-1, 0)$ and $(+1, 0)$, is the xz
259 plane and the $\pi - \sigma$ representation reduces to the standard TM/TE

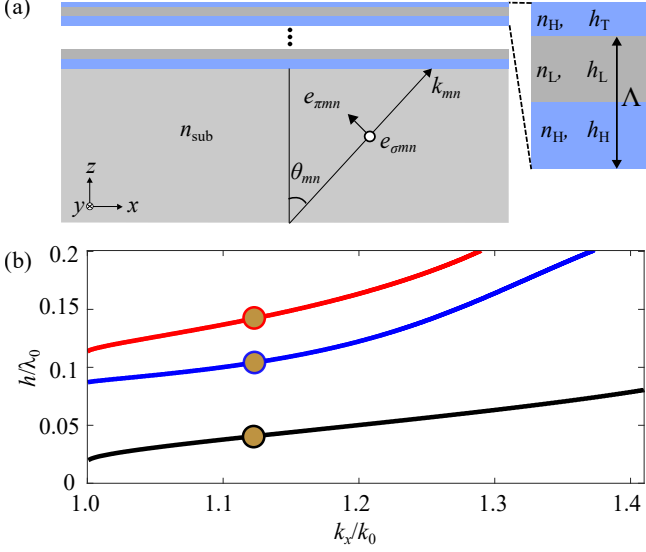


Figure 3: (a) Definition of the multilayer structure and notation. (b) Stack parameters as a function of the ratio $k_x/k_0 = n_{\text{eff}}$ for TE-mode BSW excitation with $N = 6$ bilayers: h_H/λ_0 (blue), h_L/λ_0 (red), and h_T/λ_0 (black). The dots mark the position $k_x/k_0 = 1.1209$ for BSW excitation at 50° angle of incidence.

decomposition. Since, by symmetry, $\eta_{-1,0} = \eta_{+1,0}$ for binary profiles defined in the inset of Fig. 1, we need to maximize $\eta_{+1,0}$. This also leads to the optimum value of $J_{\sigma\sigma mn}$, while $J_{\pi\pi mn} = 0$. Now we only need to find the values of the fill factor $f = c/\lambda_0$ and grating height h/λ_0 that maximize $\eta_{+1,0}$ ($= \eta_{-1,0}$) to also maximize $J_{\sigma\sigma}$.

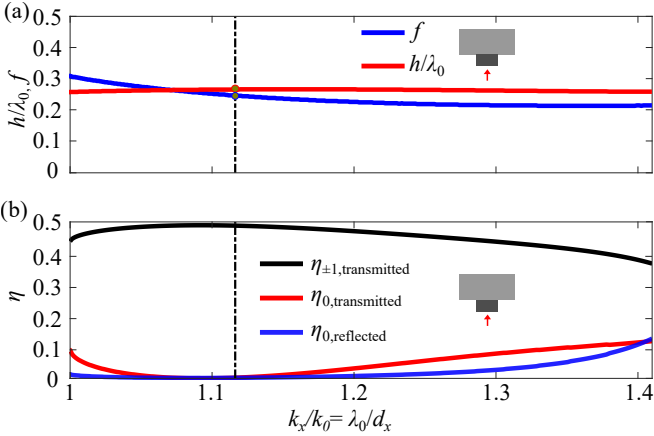


Figure 4: Design of two-way beam splitters. (a) Optimum values of the fill factor f (red) and the relief depth h/λ_0 (blue) as a function of the exit angle of the first diffracted order in TE polarization. (b) The corresponding first-order diffraction efficiency $\eta_{+1,0} = \eta_{-1,0}$ (black), the efficiency $\eta_{0,0}$ of the zeroth transmitted order (red), and that of the zeroth reflected order (blue), which is $1 - 2\eta_{+1,0} - \eta_{0,0}$ due to energy conservation. The inset shows the grating structure and direction of illumination.

The grating-design results are summarized in Fig. 4(a). The optimum fill factor remains fairly constant over the entire angular range considered here, whereas the optimum grating height decreases with increasing angle. The efficiencies of all propagating orders are plotted in Fig. 4(b). At around $k_x/k_0 = 1.1209$ (corresponding to an excitation angle 50°) we get $\eta_{\pm 1,0} \approx 0.4973$. Some

light is ‘lost’ in zeroth reflected and transmitted orders when we move close to the cut-off at $k_x/k_0 = 1$ or towards larger values of k_x/k_0 , but the designs remain acceptable over a relatively wide range of excitation angles.

The results in Figs. 3(b) and 4 allow us to design two-way beam splitters for any BSW resonance angle of interest. The stack design for the desired angle is obtained from Fig. 3(b) and the corresponding grating design from Fig. 4(a). The performance of the design can be evaluated from Fig. 4(b). To limit the number of variables further, we set $\theta_{\text{BSW}} = 50^\circ$, corresponding to $k_x/k_0 = 1.1209$. The stack design is marked by the dots in Fig. 3(b), the optimum parameters for TE excitation with $N = 6$ bilayers being $h_H = 60$ nm, $h_L = 85$ nm, and $h_T = 20$ nm. Correspondingly, the vertical lines in Fig. 4(a) give a grating design $f = 0.2536$, $h/\lambda_0 = 0.2752$, with $\eta_{\pm 1,0} = 0.4973$.

Considering the optimized case represented by the dots on Fig. 3 and the black dashed line on Fig. 4, simulation of the reflected and transmitted coefficients has been performed for the full structure. It implies a grating of period $d \simeq 459$ nm and fill factor is $f = 0.2536$ and $h/\lambda_0 = 0.2752$ on the lower side of a $10\text{-}\mu\text{m}$ -thick fused silica wafer on top of which the multilayer is deposited. The multilayer design leads to a Bloch surface wave excited when the first diffracted order emerge from the grating at an angle of 50° ($k_x/k_0 = 1.1209$) at a wavelength of 514 nm. This is observed in Fig. 5(a), where a strong dip in reflection arises at this value of k_x/k_0 . In Fig. 5(b) the response in wavelength is presented. One can observe a relatively strong peak in transmission slightly shifted with regards to the reflection dip.

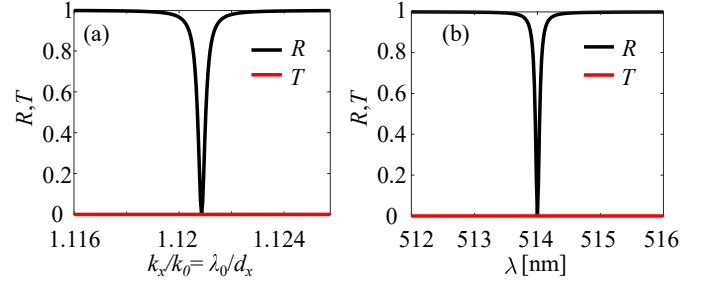


Figure 5: Response of the full structure (grating, substrate, multilayer and superstrate). (a) and (b) Reflected (black curves) and transmitted (red curves) first diffracted orders as a function of the normalized wavevector (a) and wavelength (b).

5 Plane-wave design with biperiodic gratings

We proceed to design of two-dimensionally periodic gratings that allow simultaneous excitation of more than two BSWs. Two lattice geometries are considered: square lattices for four-way excitation and hexagonal lattices for six-way excitation.

307 5.1 Four-way splitting

308 Let us first consider biperiodic gratings with primitive direct-
 309 lattice vectors $\mathbf{a}_1 = d\hat{x}$, $\mathbf{a}_2 = d\hat{y}$. The (Wigner–Seitz) primi-
 310 tive cell is square-shaped, covering the area $-d/2 < x < d/2$,
 311 $-d/2 < y < d/2$. The spatial frequencies of the diffraction or-
 312 ders are then $k_{xm} = mK$, $k_{yn} = nK$, the coordination number
 313 is 4, and the nearest neighbors of the zeroth order $(0, 0)$, namely
 314 $(m, n) = (+1, 0)$, $(0, +1)$, $(-1, 0)$, $(0, -1)$, propagate in direc-
 315 tions $\phi_{+1,0} = 0$, $\phi_{0,+1} = \pi/2$, $\phi_{-1,0} = \pi$, $\phi_{0,-1} = 3\pi/2$, re-
 316 spectively. By an appropriate choice of d , all of these four orders
 317 can be placed simultaneously on the yellow ring in Fig. 2(a), thus
 318 enabling four-way BSW excitation.

319 In the design, we found it sufficient to consider binary (z -invariant)
 320 relative-permittivity profiles of the particular form

$$\epsilon_r(x, y, z) = \begin{cases} n_1^2 & \text{when } x^2 + y^2 < r^2 \\ n_2^2 & \text{otherwise} \end{cases} \quad (18)$$

321 in $0 < z < h$ within the primitive cell. The circular feature defined
 322 by the radius r can be either a pillar ($n_1 = n_{\text{sub}}$, $n_2 = 1$ or a
 323 hole ($n_1 = 1$, $n_2 = n_{\text{sub}}$) etched in the substrate. This type of pil-
 324 lar/hole structures can be patterned at a nanometer-scale addressing
 325 resolution using electron beam lithography system available to us,
 326 and require only a single etching step.

327 The radius r and the relief depth h can be used as the structural
 328 design parameters. Some symmetry rules exist, which are helpful
 329 in the design. Since the unit cell and the structure are centered at the
 330 origin, the transmission coefficients in Eq. (8) satisfy the inversion
 331 symmetry rules

$$T_{x,-m,-n} = T_{xmn}, \quad T_{y,-m,-n} = T_{ymn}, \quad (19)$$

332 for both (x) and (y) input polarizations. These rules hold regard-
 333 less of the input polarization state, which however has an effect on
 334 the actual values of T_{xmn} and T_{ymn} . They reduce the number of
 335 orders that we need to (or can) control from four to two: we see
 336 from Eq. (19) that $\eta_{-m,-n} = \eta_{mn}$. Similar symmetry rules hold
 337 also for $J_{\sigma\sigma mn}$ and $J_{\pi\pi mn}$.

338 We begin the design of four-way couplers by optimizing the struc-
 339 tural parameters r and h to minimize the sum of the efficiencies
 340 of the reflected and transmitted zeroth orders. This maximizes the
 341 combined efficiency of the four nearest-neighbor diffraction orders,
 342 and leaves the polarization state of the incident field free for design.
 343 Choosing $\theta_{\text{BSW}} = 50^\circ$ ($d \approx 0.892\lambda_0$), for either 45° or circu-
 344 larly polarized illumination and considering pillars, we get a design
 345 $r \approx 0.201\lambda_0$, $h \approx 0.53176\lambda_0$, which gives reflected and transmit-
 346 ted zero-order efficiencies of $\sim 3.5\%$ and $\sim 5.2\%$, respectively,
 347 leaving the rest of the incident energy to be distributed among the
 348 nearest-neighbor orders.

349 Our remaining target is to equalize (and maximize) the coupling
 350 strengths $J_{\sigma\sigma mn}$ of the four signal orders by designing the input
 351 polarization state defined in Eq. (7). The symmetry in the 4-way

352 splitting implies that there is no structurally induced polarization
 353 conversion: for (x)-polarized input we get $J_{\sigma\sigma mn} = 0$ for orders
 354 $(m, n) = (\pm 1, 0)$, while (y)-polarized input gives $J_{\sigma\sigma mn} = 0$
 355 for orders $(m, n) = (0, \pm 1)$. Considering linearly polarized light,
 356 the values of $J_{\sigma\sigma mn}$ (and $J_{\pi\pi mn}$) vary rapidly with the angle α .
 357 Choosing $\alpha \approx \pi/4$ gives values $J_{\sigma\sigma mn} \approx 0.063$ and $\kappa_{mn} \approx 0.359$
 358 for all four orders. The same result is obtained also for circularly
 359 polarized illumination with $\alpha \approx \pi/4$, $\delta = \pm\pi/2$. Both the opti-
 360 mized diffracted efficiencies and the maximized coupling strengths
 361 occur at the same illumination polarization.

362 Considering unpolarized illumination, the matrix $\mathbf{J}_{\pi\sigma mn}$ becomes
 363 diagonal and the degree of polarization takes the form

$$P_{mn} = |s_{1mn}| = \frac{|J_{\pi\pi mn} - J_{\sigma\sigma mn}|}{J_{\pi\pi mn} + J_{\sigma\sigma mn}}. \quad (20)$$

364 With the present numerical values we obtain $P_{mn} \approx 0.473$ for all
 365 nearest-neighbor orders. Even though the excitation wave is parti-
 366 tially polarized, we obtain the same values of $J_{\sigma\sigma mn}$ as above;
 367 both of the two mutually uncorrelated components of the incident
 368 field contribute to TE-mode BSW excitation.

370 5.2 Six-way splitting

371 Let us consider a grating with hexagonal symmetry, which allows
 372 simultaneous excitation of six BSWs. The primitive vectors are
 373 now $\mathbf{a}_1 = d\hat{x}$ and $\mathbf{a}_2 = (d/2)\hat{x} + (\sqrt{3}d/2)\hat{y}$, and the Wigner–
 374 Seitz primitive cell is a hexagon as shown in Fig. 6(a). It will,
 375 however, be convenient for our purposes to define a rectangular
 376 direct-lattice cell as in Ref. [20], which covers the spatial region
 377 $-d/2 < x < d/2$, $-\sqrt{3}d/2 < y < \sqrt{3}d/2$ in Fig. 6(a). This
 378 alternative lattice representation simplifies the visualization of the
 379 geometry. It also allows the use of FMM in a cartesian instead of
 380 a non-orthogonal basis, as in Ref. [20], though in the present work
 381 we actually used the latter basis.

382 The spatial-frequency structure defined by the reciprocal-lattice
 383 primitive vectors $\mathbf{b}_1 = K\hat{x} - (K/\sqrt{3})\hat{y}$, $\mathbf{b}_2 = (2K/\sqrt{3})\hat{y}$ with
 384 $K = 2\pi/d$ is illustrated in Fig. 6(b), where the solid green circles
 385 show the locations of the allowed orders in the cartesian (k_x, k_y)
 386 system. The empty circles represent the orders of the rectangular
 387 spatial lattice, which are forbidden by the hexagonal symmetry.
 388 The yellow circle connects the six nearest neighbors of the ze-
 389 roth order that satisfy the condition for BSW excitation simulta-
 390 neously: orders $(m, n) = (+1, +1)$, $(0, +2)$, $(-1, +1)$, $(-1, -1)$,
 391 $(0, -2)$, $(+1, -1)$ of the rectangular lattice, with exit planes at an-
 392 gles $\pi/6 + q\pi/3$, $q = 0, \dots, 5$. The excited BSWs propagate along
 393 the surface of the stack in these directions.

394 In hexagonal lattice geometry, the symmetry rules in Eq. (19) en-
 395 sure $J_{\sigma\sigma,-1,-1} = J_{\sigma\sigma,1,1}$, $J_{\sigma\sigma,0,-2} = J_{\sigma\sigma,0,2}$, $J_{\sigma\sigma,-1,1} =$
 396 $J_{\sigma\sigma,1,-1}$. These symmetries leave us three pairs of orders to con-
 397 trol, and we expect to need additional structural freedom compared
 398 to the 4-wave case. Let us nevertheless see what designs are pos-

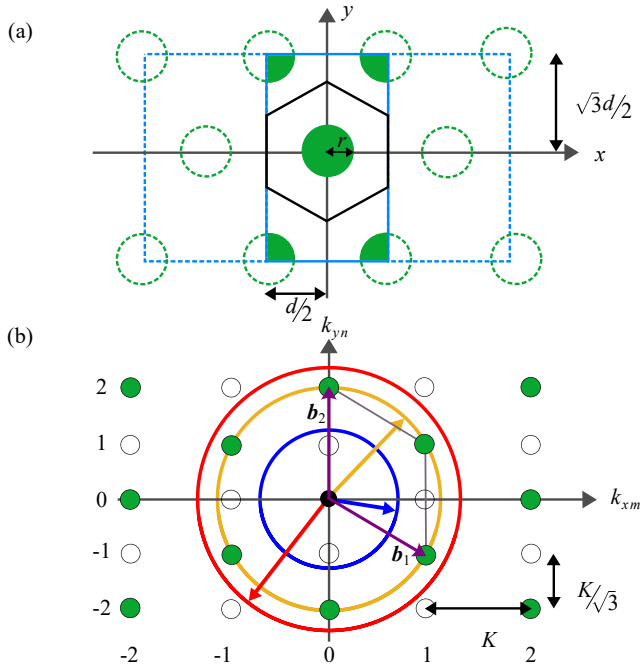


Figure 6: (a) The spatial structure of a hexagonal grating. The hexagon shows the spatial Wigner-Seitz primitive cell, the green features illustrate the grating structure, and the blue rectangle shows the non-primitive cartesian cell. (b) The spatial-frequency grid. The filled and empty dots represent the allowed and forbidden orders of the hexagonal lattice. The blue, yellow, and red circles have the same meaning as in Fig. 2(a).

399 sible with circular pillars by following the same strategy as above.
 400 An important difference is that in the hexagonal geometry we do
 401 have structurally induced polarization conversion.

402 By optimizing r and h for pillars, we get $h \approx 0.422\lambda_0$ and
 403 $r \approx 0.254\lambda_0$, which leaves a combined efficiency of ~ 0.884
 404 available for the 6 orders of interest. The distribution of $J_{\sigma\sigma mn}$
 405 again depends on input polarization. We found that it is not possi-
 406 ble to equalize the coupling exactly for all six orders, but using
 407 circularly polarized light with $\alpha = \pi/4$ and $\delta = 0.486\pi$ we have
 408 $J_{\sigma\sigma,1,1} = 0.097$, $J_{\sigma\sigma,0,2} = 0.102$, and $J_{\sigma\sigma,1,-1} = 0.113$, respec-
 409 tively. Similarly, for κ_{mn} , we have $\kappa_{1,1} = 1.691$, $\kappa_{0,2} = 1.903$,
 410 and $\kappa_{1,-1} = 2.310$. Though it is not of concern for the present
 411 purposes, it is worth noting that the diffraction efficiencies are:
 412 $\eta_{1,1} \approx 0.152$, $\eta_{0,2} \approx 0.145$, and $\eta_{1,-1} \approx 0.144$. As with the
 413 four-wave case, the design with circular pillars works also for cir-
 414 cularly polarized or unpolarized illumination but the exact values
 415 of $J_{\sigma\sigma mn}$ depend on polarization, but are within the same range as
 416 above. For unpolarized illumination, the degrees of polarization of
 417 the individual orders are nearly equal, $P_{mn} \approx 0.3226$.

418 In Fig. 7, we show the field amplitude distribution associated with
 419 the six-way coupling geometry in the xz -plane, i.e., crossing the
 420 multilayer, when illuminated with a 45° polarized light wave.
 421 The field is evaluated over 3-unit cells, i.e., 3 grating periods, in
 422 the x -direction. It shows, as expected, a strong field on the upper
 423 medium, which such structure ideal for sensing applications, espe-

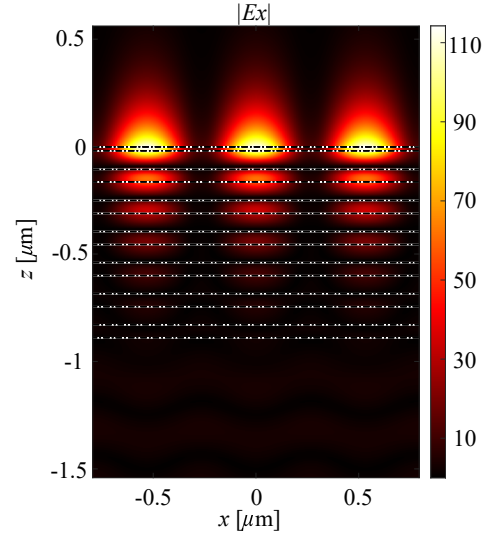


Figure 7: Field amplitude distribution across the multilayer (xz -plane). The illumination polarization was set to 45° . The dashed lines superimposed on the field represent the multilayer interfaces.

424 cially when providing multiple sensing areas thanks to the splitting
 425 of the BSW excitation.

426 6 Discussion

427 Throughout the paper we have considered normally incident illu-
 428 mination. The use of non-normal incidence could potentially allow
 429 us to consider other combinations of diffracted orders being simul-
 430 taneously resonant. Changing the angle of incidence moves the grid
 431 of diffracted orders transversely in Fig. 2(a) with respect to the cir-
 432 cles centered at the origin. For instance, if the propagation direction
 433 of the incident field is chosen as $(k_{x1}, k_{y1}) = (0, k_{y1})$, increasing
 434 k_{y1} moves the grid downwards in k_y direction, giving the orders at
 435 positions $k_{xm} = mK_x$, $k_{yn} = k_{y1} + nK_y$. Hence the three orders
 436 $(m, n) = (0, 0)$ and $(m, n) = (\pm 1, 0)$ would have a common ra-
 437 dial spatial frequency if $k_{y1} = -(K_x^2 + K_y^2)/2K_y$, being therefore
 438 available for 3-way BSW excitation. To avoid order $(0, 2)$ from oc-
 439 cupping the same ring as the zeroth order, we would need to choose
 440 $K_x \neq K_y$. However, placing the (yellow) BSW resonance ring out-
 441 side the blue ring in Fig. 2(a) requires $k_{\rho 00} > k_0 n_{\text{sub}}$, which is not
 442 possible with incidence from air. Hence a Kretschmann excitation
 443 geometry would be needed, thus sacrificing the compact footprint
 444 of the setup.

445 As an alternative to the geometry considered in this paper, we could
 446 consider having the splitter grating and the BSW stack as an inte-
 447 grated structure. This would still allow a compact platform at nor-
 448 mal incidence, but the grating design and BSW stack design would
 449 not be independent anymore. As a first drawback, the splitter grat-
 450 ing would most likely have to be rather thick ($\sim \lambda_0$) to suppress
 451 the zeroth transmitted order, preventing the possibility of etching it
 452 in the top ML layer. As a consequence, a strong degrading effect
 453 in the excited BSWs would be expected. Alternatively, one could
 454 use a highly index-modulated splitter grating with a flat top sur-
 455 face immediate below the stack. This would partially alleviate the

456 dependency in the ML and the grating design, but presumably the
457 BSWs would be less affected.

458 7 Conclusions

459 In summary, we considered grating design for 2-way, 4-way, and
460 6-way BSW coupling at normally incident but arbitrarily polarized
461 illumination of gratings with linear, square, and hexagonal symme-
462 tries. The plane-wave designs feature ideal TE-mode BSW cou-
463 pling in the two-wave case. In the other cases the non-resonant
464 parts of the excitation orders cannot be eliminated simultaneously,
465 and they actually dominate the resonant (σ polarized) parts by a
466 factor of ~ 2.8 in the 4-wave case. The 6-wave case reveals the
467 opposite observation with the resonant part dominating by a factor
468 of ~ 1.968 making them ideal candidate for TE-mode BSW exci-
469 tation. Nevertheless, in the 4-wave case all four coupling ratios can
470 be made equal, and in the 6-wave case practically equal, for several
471 input polarization states of practical significance.

472 Funding

473 The work was partially funded by the Academy of Finland through
474 project 333938 and the Flagship Program PREIN (346518). E. De-
475 scrovi acknowledges the funding received by Italian “Ministero
476 dell’Università e della Ricerca” under the “Dipartimento di Eccel-
477 lenza 2018-2022” program.

478 Disclosures

479 The authors declare no conflicts of interest.

480 REFERENCES

481 [1] W. M. Robertson, M. S. May, “Surface electromagnetic
482 wave excitation on one-dimensional photonic band-gap
483 arrays,” *Appl. Phys. Lett.* **74**, 1800–1802 (1999).
484 [2] M. Liscidini, J. E. Sipe, “Enhancement of diffraction for
485 biosensing applications via Bloch surface waves,” *Appl.*
486 *Phys. Lett.* **91**, 253125 (2007).
487 [3] F. Villa and J. A. Gaspar-Armenta, “Photonic crystal to
488 photonic crystal surface modes: narrow-bandpass filters,”
489 *Opt. Express* **12**, 2338–2355 (2004).
490 [4] E. Moggi, G. Pellegrini, J. Gil-Rostra, F. Yubero, G. Si-
491 mone, S. Fossati, J. Dostálek, R. Martínez Vázquez, R.
492 Osellame, M. Celebrano, M. Finazzi, P. Biagioni, “One-
493 dimensional photonic crystal for surface mode polariza-
494 tion control,” *Adv. Opt. Mater.* 2200759 (2022).
495 [5] A. L. Asilevi, H. Pesonen, S. Pelisset, E. Descrovi,
496 M. Roussey, and J. Turunen, “Pulse modulation by

497 Bloch Surface Wave excitation,” *Opt. Lett.* **47**, 2574–2577
498 (2022).

499 [6] E. Descrovi, F. Frascella, B. Sciacca, F. Geobaldo, L.
500 Dominici, F. Michelotti, “Coupling of surface waves in
501 highly defined one-dimensional porous silicon photonic
502 crystals for gas sensing applications,” *Appl. Phys. Lett.*
503 **91**, 241109 (2007).
504 [7] D. N. Gulkin, A. A. Popkova, B. I. Afinogenov, D. A.
505 Shilkin, K. Kuršelis, B. N. Chichkov, V. O. Bessonov,
506 A. A. Fedyanin, “Mie-driven directional nanocoupler for
507 Bloch surface wave photonic platform,” *Nanophotonics*
508 **10**, 2939–2947 (2021).
509 [8] M. Wang, H. Zhang, T. Kovalevich, R. Salut, M.-S. Kim,
510 M. A. Suarez, M.-P. Bernal, H.-P. Herzig, H. Lu, T. Gros-
511 jean, “Magnetic spin-orbit interaction of light,” *Light Sci.*
512 *Appl.* **7**, 24 (2018).
513 [9] R. Wang, H. Xia, D. Zhang, J. Chen, L. Zhu, Y. Wang, E.
514 Yang, T. Zang, Tianyang, X. Xiaolei, G. Zou, P. Wang, H.
515 Ming, R. Badugu, J. R. Lakowicz, “Bloch surface waves
516 confined in one dimension with a single polymeric nanofi-
517 bre,” *Nat. Commun.* **8**, 14330 (2017).
518 [10] K. R. Safronov, V. O. Bessonov, D. V. Akhremenkov, M.
519 A. Sirotin, M. N. Romodina, E. V. Lyubin, I. V. Sobol-
520 eva, A. A. Fedyanin, “Miniature Otto prism coupler for
521 integrated photonics,” *Laser & Photonics Reviews*, **16**,
522 2100542 (2022).
523 [11] E. A. Bezus, D. A. Bykov, L. L. Doskolovich, “Integrated
524 diffraction gratings on the Bloch surface wave platform
525 supporting bound states in the continuum,” *Nanopho-*
526 *tonics* **10**, 4331–4340 (2021).
527 [12] T. Kovalevich, P. Boyer, M. Suarez, R. Salut, M.-S.
528 Kim, H. P. Herzig, M.-P. Bernal, T. Grosjean, “Polariza-
529 tion controlled directional propagation of Bloch surface
530 wave,” *Opt. Express* **25**, 5710 (2017).
531 [13] M. Scaravilli, A. Micco, G. Castaldi, G. Coppola, M.
532 Giofrè, M. Iodice, V. La Ferrara, V. Galdi, A. Cusano,
533 “Excitation of Bloch surface waves on an optical fiber
534 tip,” *Adv. Opt. Mater.* **6**, 1800477 (2018).
535 [14] V. Koju, W. M. Robertson, “Leaky Bloch-like surface
536 waves in the radiation-continuum for sensitivity en-
537 hanced biosensors via azimuthal interrogation,” *Sci. Rep.*
538 **7**, 3233 (2017).
539 [15] M. Scaravilli, G. Castaldi, A. Cusano, V. Galdi, “Grating-
540 coupling-based excitation of Bloch surface waves for lab-
541 on-fiber optodes,” *Opt. Express* **24**, 27771 (2016).
542 [16] R. Wang, X. Lei, Y. Jin, X. Wen, L. Du, A. Wu, A. V.
543 Zayats, X. Yuan, “Directional imbalance of Bloch sur-
544 face waves for ultrasensitive displacement metrology,”
545 *Nanoscale* **13**, 11041–11050 (2021).
546 [17] C.-Z. Deng, Y.-L. Ho, H. Yamahara, H. Tabata, J.-J. De-
547 launay, “Near-Zero-Index Slabs on Bloch Surface Wave
548 Platform for Long-Range Directional Couplers and Op-
549 tical Logic Gates,” *ACS Nano* **16**, 2224–2232 (2022).
550 [18] X. Lei, R. Wang, L. Liu, C. Xu, A. Wu, Q. Zhan, “Mul-
551 tifunctional on-chip directional coupler for spectral and
552 polarimetric routing of Bloch surface wave,” *Nanopho-*

- 553 tonics, doi:10.1515/nanoph-2022-0397 (2022).
- 554 [19] H. Kim, J. Park, and B. Lee, *Fourier Modal Method and*
555 *it Applications in Computational Nanophotonics* (CRC
556 Press, 2012).
- 557 [20] E. Noponen and J. Turunen, “Eigenmode method for
558 electromagnetic synthesis of diffractive elements with
559 three-dimensional profiles,” *J. Opt. Soc. Am. A* **11**, 2494–
560 2502 (1994).
- 561 [21] J. Tervo, I. A. Turunen, and B. Bai, “A general approach
562 to the analysis and description of partially polarized light
563 in rigorous grating theory,” *J. Eur. Opt. Soc: Rapid Publ.*
564 **3**, 08004 (2008).
- 565 [22] L. Mandel and E. Wolf, *Optical Coherence and Quantum*
566 *Optics* (Cambridge, 1995).
- 567 [23] K. R. Safronov, D. N. Gulkin, I. M. Antropov, K.
568 A. Abrashitova, V O. Bessonov, and A. A. Fedyanin,
569 “Multimode interference of Bloch surface electromagnetic
570 waves,” *ACS Nano* **14**, 10428–10437 (2020).
- 571 [24] R. Dubey, B. V. Lahijani, E. Barakat, M. Häyrynen, M.
572 Roussey, M. Kuittinen, H. P. Herzig, “Near-field char-
573 acterization of a Bloch-surface-wave-based 2D disk res-
574 onator,” *Opt. lett.* **41**, 4867–4870 (2016).